Interactions Between Two Phase-locked Loop Synchronized Grid Converters

Zou, Zhixiang; Besheli, Behnam Daftary; Rosso, Roberto; Liserre, Marco; Wang, Xiongfei

Published in:
IEEE Transactions on Industry Applications

DOI (link to publication from Publisher):
10.1109/TIA.2021.3081611

Publication date:
2021

Document Version
Accepted author manuscript, peer reviewed version

Interactions Between Two Phase-locked Loop Synchronized Grid Converters

Zhixiang Zou, *Senior Member, IEEE,* Behnam Daftary Besheli, Roberto Rosso, *Student Member, IEEE,* Marco Liserre, *Fellow, IEEE* and Xiongfei Wang, *Senior Member, IEEE*

***Abstract*—Grid converters synchronized by phase-locked loops (PLLs) could suffer from stability problems, especially being connected to a weak grid or high penetration of converters. The existing literature assesses the stability of the paralleled PLL-synchronized converters at the same point of common coupling (PCC) using identical control and system parameters. However, in an actual grid, the parameters of grid converters are normally different due to different manufacturers. In this regard, this paper aims to study the stability indices and margins of two PLL-synchronized converters with different parameters, particularly with different PLL bandwidths and power injections. The main purpose of this paper is to provide a general design guidelines of PLL bandwidths of two converters (can be extended to two wind/solar farms) for stable operation in practical grids. State-space model of the PLL-synchronized converter based on the component connection method (CCM) is developed and eigenvalue-based analysis is used to investigate the interactions between the two converters. Moreover, the stability borders of two PLL-synchronized converters using different PLL bandwidths and power setpoints are studies. Monte-Carlo simulations and experimental results are provided to validate the effectiveness of the developed model and theoretical analysis.**

***Index Terms*—Grid converter, synchronization, phase-locked loop (PLL), stability analysis, Monte-Carlo analysis.**

NOMENCLATURE

P_{ref}	Active power setpoint of grid converter
Q_{ref}	Reactive power setpoint of grid converter
θ	Phase angle of SRF-PLL
$\Delta\theta$	Phase displacement between actual grid and PLL
$v_{PCC,d}$	d-axis PCC voltage seen by dq frame of grid
$v_{PCC,q}$	q-axis PCC voltage seen by dq frame of grid
$v^m_{PCC,d}$	d-axis PCC voltage seen by dq frame of PLL
$v^m_{PCC,q}$	q-axis PCC voltage seen by dq frame of PLL
$v_{r,d}$	d-axis reference voltage seen by dq frame of grid
$v_{r,q}$	q-axis reference voltage seen by dq frame of grid
$v^c_{r,d}$	d-axis reference voltage seen by dq frame of PLL
$v^c_{r,q}$	q-axis reference voltage seen by dq frame of PLL
v_g	Equivalent voltage of slack bus
i_{dref}	d-axis current reference of grid converter
i_{qref}	q-axis current reference of grid converter
$i_{con,d}$	d-axis converter current seen by dq frame of grid
$i_{con,q}$	q-axis converter current seen by dq frame of grid
$i^m_{con,d}$	d-axis converter current seen by dq frame of PLL
$i^m_{con,q}$	q-axis converter current seen by dq frame of PLL
$i_{g,d}$	d-axis grid current
$i_{g,q}$	q-axis grid current
$i_{L,d}$	d-axis load current
$i_{L,q}$	q-axis load current
T_s	Sampling period
γ	State variable of PI controller of PLL
ϵ_d	State variable of d-axis current controller
ϵ_q	State variable of q-axis current controller
σ_n	Real part of the n-th eigenvalue
ω_n	Imaginary part of the n-th eigenvalue
ζ_{dn}	Damping ratio of the n-th eigenvalue
f_{BW}	PLL bandwidth
BW_{con1}	PLL bandwidth of Converter 1
BW_{con2}	PLL bandwidth of Converter 2
$BW_{limit,2p.u.}$	Critical PLL bandwidth of two converters with 2 p.u. power injection
ΔBW_{con1}	Deviation between BW_{con1} and $BW_{limit,2p.u.}$
ΔBW_{con2}	Deviation between BW_{con2} and $BW_{limit,2p.u.}$

Z. Zou is with the School of Electrical Engineering, Southeast University, 210096 Nanjing, China (e-mail: zzou@seu.edu.cn).

B. D. Besheli is with the LAWI Engineering GmbH, 24118 Kiel, Germany.

R. Rosso is with the ENERCON GmbH, 26607 Aurich, Germany.

M. Liserre is with the Chair of Power Electronics, Kiel University, 24143 Kiel, Germany.

X. Wang is with the Department of Energy Technology, Aalborg University, 9220 Aalborg, Denmark.

Manuscript received October 26, 2020; revised March 21, 2021.

This work was supported in part by the National Natural Science Foundation of China under Grant 52007033 and in part by Jiangsu Provincial Key Laboratory of Smart Grid Technology and Equipment, Southeast University.

I. INTRODUCTION

MOST of power converters are to be equipped with PLL-based synchronization to preserve the phase shift and phase sequencing during grid-connected operation [1]. In case of low penetration of grid converters, the impact of PLL on the grid is negligible comparing to the inertia response of other power system components [2]. However, when increasing the penetration of converters, the effect of grid synchronization could lead to misjudgment of the grid characteristics as well as stability [3], [4]. For this reason, the stability problems associated with the grid synchronization have been widely studied in the literature.

The previous research efforts in this topic are mainly focusing on the modeling and stability analysis of PLL-synchronized converter(s) in a weak grid. One method to accurately deal with grid converter and its synchronization is to use impedance-based model, which are derived from the small-signal modeling technique in the frequency-domain [5]. In [6], the input admittance by introducing the effect of PLL has been studied and it shows that the high bandwidth PLL enhances the negative real part of the converter admittance, which compromises the system stability. Later on, impedance models including the effect of the PLL are developed in both the synchronous reference frame and the stationary frame, respectively [7], [8], [9]. Design methods considering the instability issue associated with PLL have been proposed in [10], [11], [12] to improve system stability.

Moreover, the impedance model of PLL-synchronized converter has been further extended in the synchronous frame for the stability analysis when incurring large phase perturbations [13], [2]. In [14], the design-oriented transient stability of PLL-synchronized converter has been investigated during grid faults.

Another method is the eigenvalue analysis based on the state-space model in the time-domain [15]. Comparing to the impedance model, though it requires high computation power, the identifications of the oscillation modes and the participation factor of system variables are superior [16]. To reduce the modeling complexity, the CCM is introduced that can reformulate conventional state-space model according to the terminal characteristic, and it is scalable for the system with a large number of grid converters [17], [18]. In [19] and [20], the detailed state-space model of a PLL-synchronized converter has been developed and the stability as well as the participation factors have been carried out using eigenvalue analysis. On this basis, the state-space model and the stability assessment of multiple grid converters have been studied in [21], [22]. In the analysis of both time-domain and frequency-domain, it is shown that the increasing of power injection of grid converters further decreases the stability margin, which leads to the upper limit of the PLL bandwidth for stable operation getting lower [23], [24].

Most of the previous works of modeling and stability analysis employ identical system and control parameters for the parallel converters. However, in an actual grid, the parameters especially the PLL bandwidth and the power setpoints of different grid converters are normally different [25]. Thus, the stability indices and margins of an actual system with different converter parameters would be distinguished from the ideal one with identical parameters. More specifically, the critical PLL bandwidth for guaranteeing stable operation derived from the ideal system would be no longer valid in a practical grid.

In this respect, this paper aims to study the stability of two PLL-synchronized grid converters with different parameters (particularly different PLL bandwidths and power setpoints) in a weak grid. To well study the problem, a state-space model based on the CCM for the eigenvalue-based analysis was firstly developed in [26], and it has been further improved and the detailed model is presented in this work. The stability indices and margins as well as the limits of PLL bandwidth for the two converters with different parameters are investigated based on the developed model. A full map indexing the stability border of a distribution grid with two converters is eventually presented in this paper, which is expected to provide a general design guideline of converter (or wind/solar farm) parameters for stable operation.

The paper structure is organized as follows. The state-space model including grid converters and LV network is developed in Section II. Based on the developed model, eigenvalue-based analysis and stability indices/borders of two converters are presented in Section III. Monte-Carlo analysis and experimental results are provided in Section IV and Section V to verify the effectiveness of the model and the theoretical analysis. Conclusions are drawn in Section VI.

II. Modeling of PLL-synchronized Grid Converters

The system configuration of grid-connected converters in parallel is shown in Fig. 1a, and the control schematic diagram of each grid converter is given in Fig. 1b. The implementation of system model by using the CCM is shown in Fig. 2.

A. Modeling of Grid Converter

The classic system configuration and control block diagram of a grid converter are shown in Fig. 1b, which is composed of an LCL-filter, a synchronous reference frame-(SRF)-PLL, the power/current controller, and the pulse width modulation (PWM). To simplify the analysis, the effect of the power control loop are neglected and the current references generated from the power loop (i.e., i_{dref} and i_{qref}) can be regarded as constant in steady state. Usually, during normal operation, it operates at unity power factor (e.g., in PV applications), namely, Q_{ref} or i_{qref} can be set as zero, while it can support the voltage profile by injecting reactive power upon the requests from the distribution system operator or by respecting grid codes. The SRF-PLL is one of the most commercially used grid synchronization techniques [27] while it affects the characteristics of variables through the Park transform and its inverse. This is due to the small-signal perturbation of grid voltage, which propagates to the PLL phase angle and then leads to two dq frames: one is the frame of the actual grid, and another is coordinated by the PLL. The phase displacement between the two frames is $\Delta\theta$. An example of PCC voltage in both dq frames is shown in Fig. 3. This can be further modeled by Fig. 4a and the formulation can be represented by

$$\begin{bmatrix} v^m_{PCC,d} \\ v^m_{PCC,q} \end{bmatrix} = \begin{bmatrix} cos\Delta\theta & sin\Delta\theta \\ -sin\Delta\theta & cos\Delta\theta \end{bmatrix} \begin{bmatrix} v_{PCC,d} \\ v_{PCC,q} \end{bmatrix} \quad (1)$$

where $v^m_{PCC,d}$ and $v^m_{PCC,q}$ are the measured d- and q-axis voltage seen by the dq frame of PLL, $v_{PCC,d}$ and $v_{PCC,q}$ are the actual d- and q-axis voltage of PCC seen by the dq frame of grid. For the converter current, a similar model can be obtained and the formulation is given by

$$\begin{bmatrix} i^m_{con,d} \\ i^m_{con,q} \end{bmatrix} = \begin{bmatrix} cos\Delta\theta & sin\Delta\theta \\ -sin\Delta\theta & cos\Delta\theta \end{bmatrix} \begin{bmatrix} i_{con,d} \\ i_{con,q} \end{bmatrix} \quad (2)$$

where $i^m_{con,d}$ and $i^m_{con,q}$ are the measured d- and q-axis current of the grid converter seen by the dq frame of PLL, $i_{con,d}$ and $i_{con,q}$ are the actual d- and q-axis current that injected to grid seen by the dq frame of grid.

The voltage reference generated by the current controller is affected by inverse transform as well as SRF-PLL. The model can be developed as shown in Fig. 4b and the formulation can be written by

$$\begin{bmatrix} v_{r,d} \\ v_{r,q} \end{bmatrix} = \begin{bmatrix} e^{-1.5T_s s} & 0 \\ 0 & e^{-1.5T_s s} \end{bmatrix} \begin{bmatrix} cos\Delta\theta & -sin\Delta\theta \\ sin\Delta\theta & cos\Delta\theta \end{bmatrix} \begin{bmatrix} v^c_{r,d} \\ v^c_{r,q} \end{bmatrix} \quad (3)$$

where

$$e^{-1.5T_s s} \approx \frac{12 - 9T_s s + 2.25(T_s s)^2}{12 + 9T_s s + 2.25(T_s s)^2} \quad (4)$$

This article has been accepted for publication in a future issue of this journal, but has not been fully edited. Content may change prior to final publication. Citation information: DOI 10.1109/TIA.2021.3081611, IEEE Transactions on Industry Applications

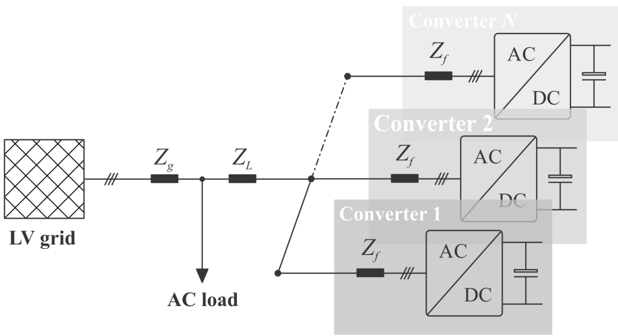

(a)

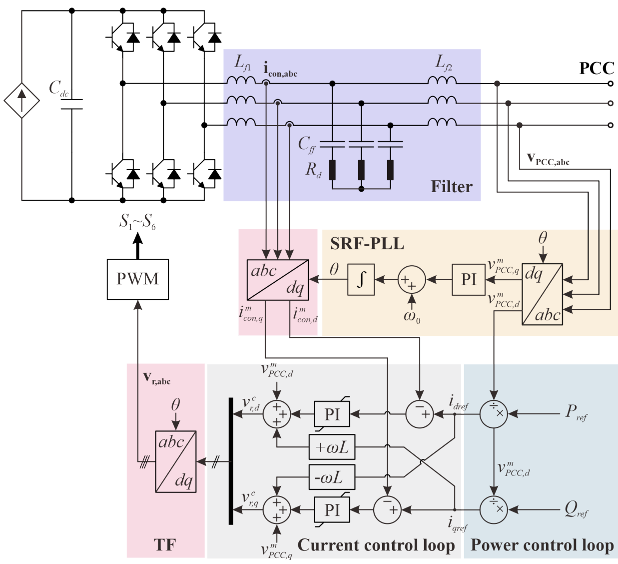

(b)

Fig. 1. Grid converters in a low voltage (LV) grid: (a) system configuration and (b) control scheme of single converter.

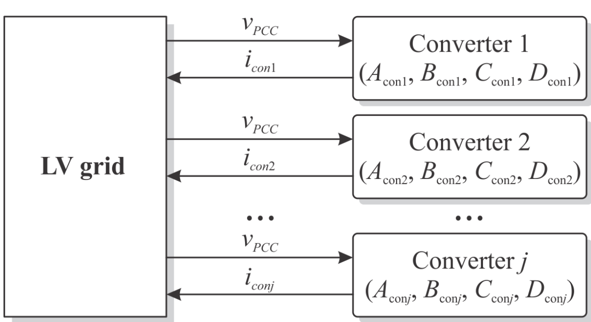

Fig. 2. CCM-based system model of grid converters in a LV grid.

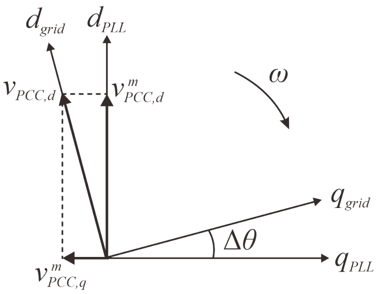

Fig. 3. dq frame of grid and the one coordinated by PLL.

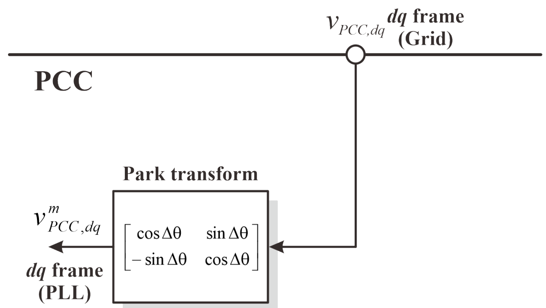

(a)

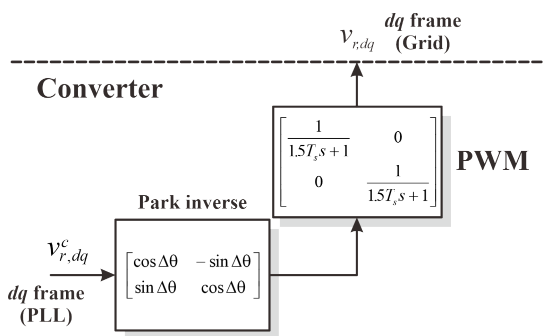

(b)

Fig. 4. Model of Park transform and its inverse in dq frame considering the effect of PLL: (a) Park transform and (b) inverse transform.

is the one-and-half sampling period delay which denotes the PWM and computational delay, and it can be approximated by the second-order Padé approximation, $v_{r,d}$ and $v_{r,q}$ are the d- and q-axis reference voltage seen by the dq frame of grid, $v^c_{r,d}$ and $v^c_{r,q}$ are the d- and q-axis voltage of the current control output (seen by the dq frame of PLL).

By combining (1)-(3), and considering the characteristics of the current controller as well as the filter, the full state-space model of a PLL-synchronized converter can be formulated by (5) and the detailed differential equations are given in the Appendix.

$$\begin{aligned}\dot{x}_{conj} &= A_{conj}x_{conj} + B_{conj}u_{conj}\\ y_{conj} &= C_{conj}x_{conj}\end{aligned} \tag{5}$$

where the subscript $_j$ indicate the j-th grid converter that connects to the PCC, the state variables of the grid converter are $x_{conj} = [v^m_{PCC,d}, v^m_{PCC,q}, \Delta\theta, \gamma, \epsilon_d, \epsilon_q, i^m_{con,d}, i^m_{con,q}, v_{r,d}, v_{r,q}, i_{con,d}, i_{con,q}]^T$ including the states of measured PCC voltage ($v^m_{PCC,d/q}$), phase deviation ($\Delta\theta$), PI controller of SRF-PLL (γ), current controller ($\epsilon_{d/q}$), measured converter current ($i^m_{con,d/q}$), voltage reference ($v_{r,d/q}$), and actual injected current ($i_{con,d/q}$); $u_{conj} = [v_{PCC,d}, v_{PCC,q}, i_{ref,d}, i_{ref,q}]^T$ is defined as the input vector of the grid converter, including actual PCC ($v_{PCC,d/q}$) and current reference ($i_{ref,d/q}$); $y_{conj} = [i_{con,d}, i_{con,q}]^T$ is selected as the output vector of each grid converter.

The full model can be simplified by assuming the converter to behave as an ideal current source [24], when the bandwidth of the current loop is designed to be much higher than that of

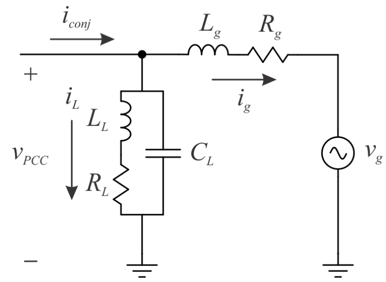

Fig. 5. Equivalent circuit of LV distribution network.

the PLL. The output current of the current source is calculated by transforming the current reference from dq to abc frame using the PLL phase angle θ. For instance, when hysteresis control is implemented, it ensures extremely high bandwidth and allows the interaction between current control and PLL to be decoupled. Nevertheless, if the current control is not fast enough, the effect of the current control cannot be removed and a full representation of (5) has to be adopted.

B. Modeling of LV Network

The equivalent circuit of a typical LV distribution network is presented in Fig. 5, and multiple grid converters are connected to the PCC of the network. Based on the equivalent circuit, the differential equations of the network can be obtained and given in the Appendix, and its state-space model can be written by

$$\begin{aligned} \dot{x}_{net} &= A_{net}x_{net} + B_{net}u_{net} \\ y_{net} &= C_{net}x_{net} \end{aligned} \tag{6}$$

where $x_{net} = [v_{PCC,d}, v_{PCC,q}, i_{g,d}, i_{g,q}, i_{L,d}, i_{L,q}]^T$ is the vector of the state variables of the LV network, including the states of PCC voltage ($v_{PCC,d/q}$), grid current ($i_{g,d/q}$), and load current ($i_{L,d/q}$); $u_{net} = [i_{conj,d}, i_{conj,q}, v_g]^T$ is the input vector of the LV network, including the output current of j-th grid converter ($i_{conj,d/q}$) and equivalent voltage of the slack bus (v_g); $y_{net} = [v_{PCC,d}, v_{PCC,q}]^T$ is selected as the output vector of the LV network.

C. Composite System Model

Combining (5) and (6), the composite system model can be described by

$$\begin{aligned} \dot{x}_{com} &= A_{com}x_{com} + B_{com}u_{com} \\ y_{com} &= C_{com}x_{com} \end{aligned} \tag{7}$$

where

$$\begin{aligned} A_{com} &= \text{diag}(A_{con1}, \ldots, A_{conj}, A_{net}) \\ B_{com} &= \text{diag}(B_{con1}, \ldots, B_{conj}, B_{net}) \\ C_{com} &= \text{diag}(C_{con1}, \ldots, C_{conj}, C_{net}) \\ x_{com} &= [x_{con1}, \ldots, x_{conj}, x_{net}]^T. \end{aligned} \tag{8}$$

According to Fig. 2, (5) and (6) can be rewritten by

$$\begin{aligned} u_{conj} &= L_{conj}y_{conj} \\ u_{net} &= L_{net}y_{net} \end{aligned} \tag{9}$$

TABLE I
SYSTEM PARAMETERS

Symbol	Quantity	Value
S_n	Grid short circuit power	1 MVA
V_g	grid voltage (phase to neutral)	230 V (rms)
L_f	filter inductance of converter	5.03 mH
R_f	filter resistance of converter	0.1 Ω
L_g	series inductance of grid	0.64 mH
R_g	series resistance of grid	0.02 Ω
L_L	shunt inductance of grid	1×10^4 H
C_L	shunt capacitance of grid	1 μF
R_L	shunt resistance of grid	2 $k\Omega$
k_p^{cc}	proportional gain of current controller	5
k_i^{cc}	integral gain of current controller	20
BW_{nom}	nominal value of PLL bandwidth	200 Hz

Combining (7) and (9), the interconnection relationship between the inputs and outputs of the components can be given by

$$u_{com} = L_{com}y_{com} \tag{10}$$

where

$$\begin{aligned} u_{com} &= [u_{con1}, \ldots, u_{conj}, u_{net}]^T \\ y_{com} &= [y_{con1}, \ldots, y_{conj}, y_{net}]^T \\ L_{com} &= \text{diag}(L_{con1}, \ldots, L_{conj}, L_{net}). \end{aligned} \tag{11}$$

Based on (6) and (10), the stability of the composite system can be assessed by the followings:

$$\dot{x}_{com} = P_{com}x_{com} \tag{12}$$

where $P_{com} = A_{com} + B_{com}L_{com}C_{com}$.

III. STABILITY ANALYSIS OF PLL-SYNCHRONIZED GRID CONVERTERS

The eigenvalue analysis of the composite system model developed in (12) will be carried out for stability assessment, using the system parameters listed in Table I. In this section, the most critical modes linked with synchronization are identified in the beginning. The relationship between the critical PLL bandwidth and the power setpoint of converter(s) are studied based on the eigenvalue analysis. The analysis is then extended to the general stability indices of two grid converters with different PLL bandwidths and power setpoints.

A. Eigenvalue and Sensitivity Analysis

The location of the 16 eigenvalues of single grid converter considering the effect of PLL is presented in Fig. 6a based on the model of (12), and a zoomed figure of the critical modes (λ_7-λ_{16}) is shown in Fig. 6b.

To investigate the sensitivity of the mode to the PLL bandwidth, a Jacobian matrix J is defined as following:

$$J(\lambda_n) = \left[\frac{\partial \sigma_n}{\partial f_{BW}}, \frac{\partial \omega_n}{\partial f_{BW}}, \frac{\partial \zeta_{dn}}{\partial f_{BW}}\right] \tag{13}$$

This article has been accepted for publication in a future issue of this journal, but has not been fully edited. Content may change prior to final publication. Citation information: DOI 10.1109/TIA.2021.3081611, IEEE Transactions on Industry Applications

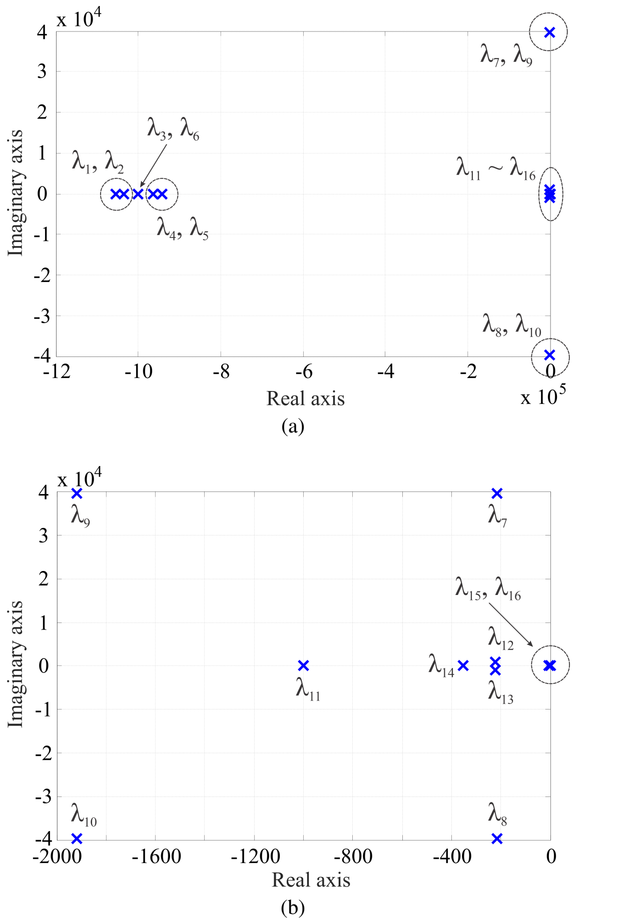

Fig. 6. Eigenvalues of single PLL-synchronized converter: (a) full eigenvalues locations and (b) zoomed eigenvalues (λ_7-λ_{16}).

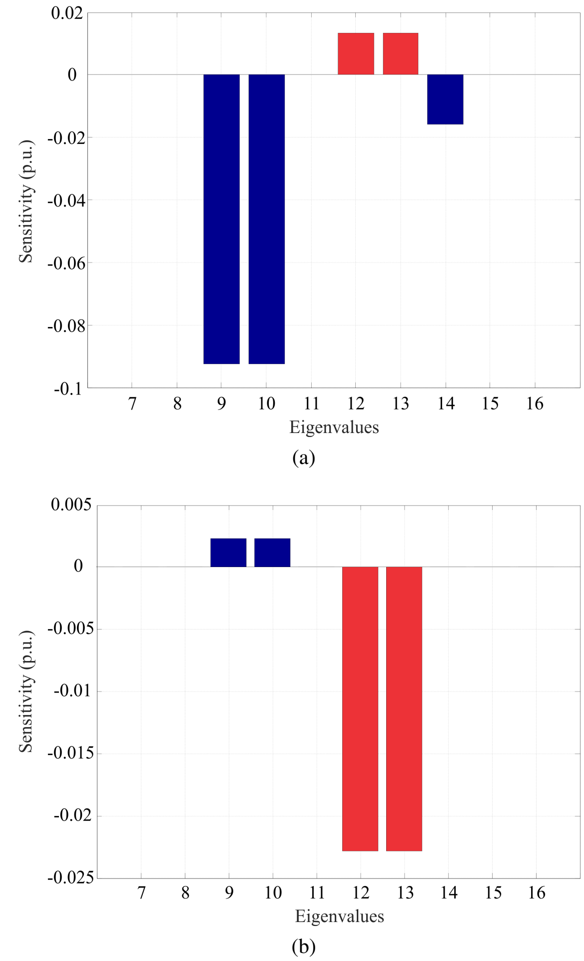

Fig. 7. Sensitivity analysis of critical modes (λ_7-λ_{16}): (a) real part σ_n and (b) damping factor ζ_{dn}.

where σ_n and ω_n are the real and the imaginary part of the n-th eigenvalue, ζ_{dn} is the damping ratio, f_{BW} indicates the PLL bandwidth. For simplicity, only the sensitivity analysis of the critical modes (i.e., λ_7-λ_{16}) are done in the followings.

The sensitivity diagrams of the critical modes to the variation of PLL bandwidth are given in Fig. 7, particularly σ_n and ζ_{dn} of each mode to the PLL bandwidth are studied. For σ_n, a bar with positive value shows a less stable condition (i.e., eigenvalue moves rightwards) when increasing the PLL bandwidth, whereas a negative bar indicates the system tends to be more stable. For ζ_{dn}, a bar with positive value indicates a system with higher damping ratio while a negative bar shows the damping ratio of the system is getting lower. From Fig. 7, it can be seen that the sensitivity of σ_{12} and σ_{13} to the PLL bandwidth variation are positive, and meanwhile the sensitivity of ζ_{d12} and ζ_{d13} to the PLL bandwidth variation are negative, showing the couple of complex conjugated poles λ_{12} and λ_{13} are the most critical modes when the PLL bandwidth increases. The rest of the eigenvalues are less sensitive to the variation of the PLL bandwidth.

B. Relationship Between Critical PLL Bandwidth and Power Setpoint

To study the relationship between the PLL bandwidth and the power setpoint (or injection), the eigenvalue trajectories of different numbers of PLL-synchronized converters have been studied and presented in Fig. 8. The first case study considers a single grid converter being connected to the PCC with 1 p.u. power injection. The PLL bandwidth increases from 0.5 p.u. till the critical modes crossing the imaginary axis, where the critical PLL bandwidth is 0.94 p.u., as shown in Fig. 8a. In the second case study, two grid converters are connected and the power injection of each is 0.5 p.u.. As seen in Fig. 8b, the system becomes unstable when the PLL bandwidth reaches 0.94 p.u. as well. It is worth noting that eigenvalue trajectories of the most critical modes (λ_{12} and λ_{13}) are overlapping of the two cases, when the total power setpoints are identical.

In an actual grid, the maximum power injection at PCC can be interpreted by the short circuit ratio (SCR) [28]. Based on the trajectories of the most critical modes, a map between the SCR and the critical PLL bandwidth is given in Fig. 9. Initially, SCR$\,=3.5$, the grid converter can maintain stable if its PLL bandwidth is low than 0.94 p.u.. When SCR$\,=2.5$, namely, the maximum allowable power injection is reduced, the PLL bandwidth has to be reduced to 0.34 p.u. to maintain stability.

This article has been accepted for publication in a future issue of this journal, but has not been fully edited. Content may change prior to final publication. Citation information: DOI 10.1109/TIA.2021.3081611, IEEE Transactions on Industry Applications

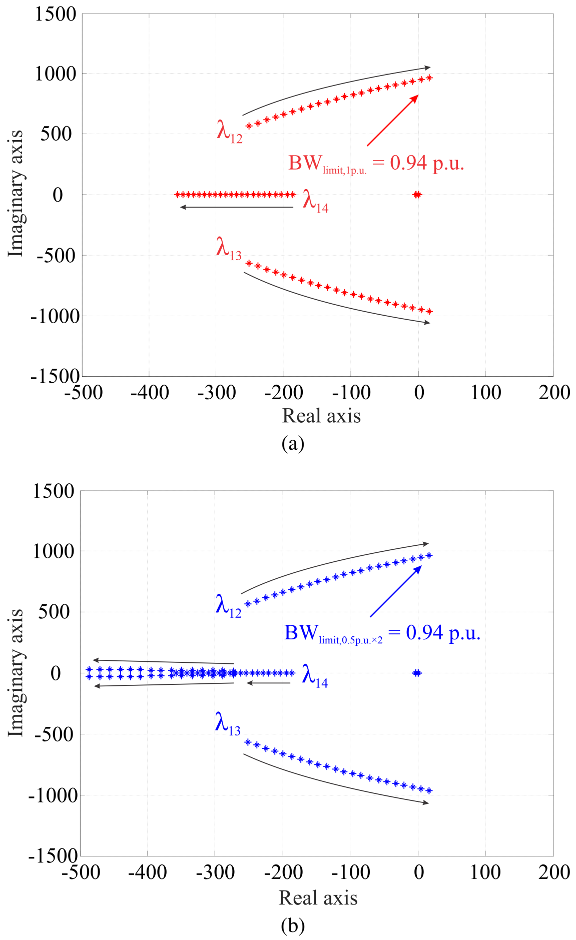

Fig. 8. Eigenvalue trajectories of grid converter(s) with nominal power setpoint(s) when changing PLL bandwidth(s): (a) single converter (1 p.u.) and (b) two converters (each 0.5 p.u.).

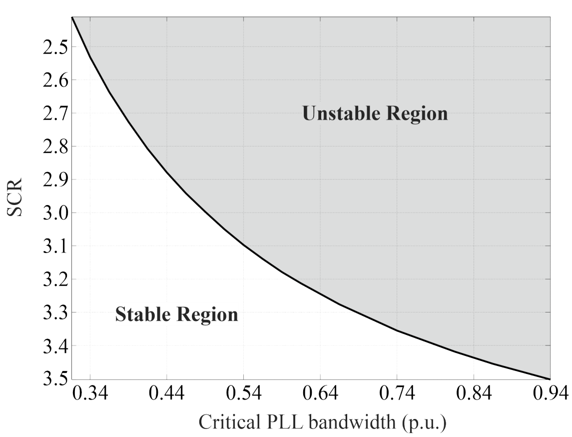

Fig. 9. Stability border regarding SCR and PLL bandwidth of grid converter.

C. Stability Analysis of Two PLL-synchronized Converters with Different Parameters

Practically, different grid converters are from different manufacturers or belong to different owners and therefore the system parameters (i.e., PLL bandwidths, power setpoints) are not always identical. To study this problem, stability analysis of two grid converters with different PLL bandwidths and power setpoints is studied in this subsection.

In the following case studies, Converter 1 with 1 p.u. power injection is connected to the PCC, which Converter 2 with 1 p.u. will be connected to. The SCR of the grid is 3.5. In case of identical parameters, the critical PLL bandwidth of the two grid converters with total 2 p.u. power injection can be defined as $BW_{limit,2p.u.}$. If the PLL bandwidth of Converter 1 (BW_{con1}) equals to $BW_{limit,2p.u.}$ (i.e., $\Delta BW_{con1} = BW_{con1} - BW_{limit,2p.u.} = 0$), the PLL bandwidth of Converter 2 (BW_{con2}) can reach up to $BW_{limit,2p.u.}$ without any stability problem (i.e., $\Delta BW_{con2} = BW_{con2} - BW_{limit,2p.u.} = 0$), as indicated by the blue eigenvalue trajectory in Fig. 10a. In this trajectory, BW_{con1} is fixed while BW_{con2} is increasing until the critical modes reach the imaginary axis. If BW_{con1} is higher than $BW_{limit,2p.u.}$, BW_{con2} has to be lower than $BW_{limit,2p.u.}$ to maintain system stability. For instance, when BW_{con1} is 0.1 p.u. higher than $BW_{limit,2p.u.}$ ($\Delta BW_{con1} = BW_{con1} - BW_{limit,2p.u.} = +0.1$ p.u.), BW_{con2} has to be at least 0.1 p.u. lower than $BW_{limit,2p.u.}$ to obtain a stable system (i.e., $\Delta BW_{con2} = BW_{con2} - BW_{limit,2p.u.} = -0.1$ p.u.), as shown by the cyan eigenvalue trajectory in Fig. 10a. Moreover, as shown by the red trajectory in Fig. 10a, when ΔBW_{con1} is $+0.5$ p.u., ΔBW_{con2} can no longer higher than -0.23 p.u. with stability concern.

In Fig. 10b, a map of the critical PLL bandwidths of two grid converters with same power setpoint is presented based on the eigenvalue analysis. In this map, BW_{con1} is higher than $BW_{limit,2p.u.}$ for all the five cases, indicating by the blue bars. To maintain stability, BW_{con2} has to be lower than $BW_{limit,2p.u.}$, which is represented by the orange bars. From case 1 to case 5, the level of the bandwidth deviations (i.e., ΔBW_{con1}, ΔBW_{con2}) gradually increases from low to high. It can be seen that the map of the critical bandwidths is symmetric when the bandwidth deviations are low, while it becomes asymmetric when the bandwidth deviations are higher. This is due to the sensitivity of the real parts of the critical modes to PLL bandwidths changes drastically. Sensitivity analysis of five case studies are carried out and the sensitivity of the real parts of the critical modes to the PLL bandwidth variations are illustrated in Fig. 10c. A blue bar with positive value indicates the real part of the critical mode moving rightwards when BW_{con1} increases, an orange bar with negative value represents the real part of the critical eigenvalue moving leftwards when decreasing BW_{con2}. When the bandwidth deviations are low, for instance in case 1, the absolute sensitivity values of both converters are very close. This leads to the absolute values of the bandwidth deviations of the two converters are close, presenting symmetric feature. On the other hand, when the bandwidth deviations are high, the absolute sensitivity value of Converter 2 is much higher than that of Converter 1. Taking case 5 as an example, even 0.2 p.u. bandwidth reduction of Converter 2 allows the bandwidth of Converter 1 increasing up to 0.4 p.u. while the system is stable.

When the power setpoints of the two converters are different, the critical PLL bandwidths would be shifted according to the power ratio of the two converters. A case study of converters with different power injections (e.g., $P_{con1}/P_{con2} = 3$)

This article has been accepted for publication in a future issue of this journal, but has not been fully edited. Content may change prior to final publication. Citation information: DOI 10.1109/TIA.2021.3081611, IEEE Transactions on Industry Applications

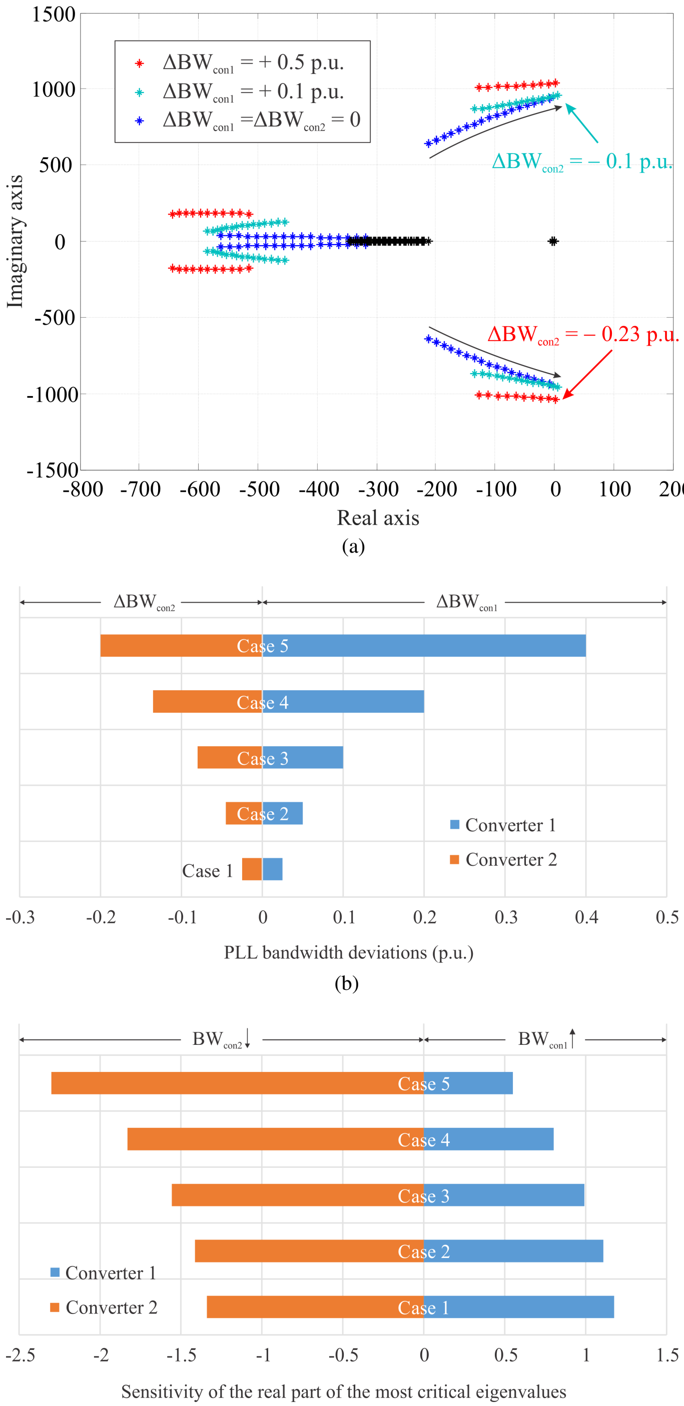

Fig. 10. Stability analysis of two PLL-synchronized converters with identical power setpoint when varying PLL bandwidths: (a) eigenvalue trajectories, (b) critical PLL bandwidths of two converters, and (c) sensitivity analysis of the real part of the most critical modes to PLL bandwidth variation.

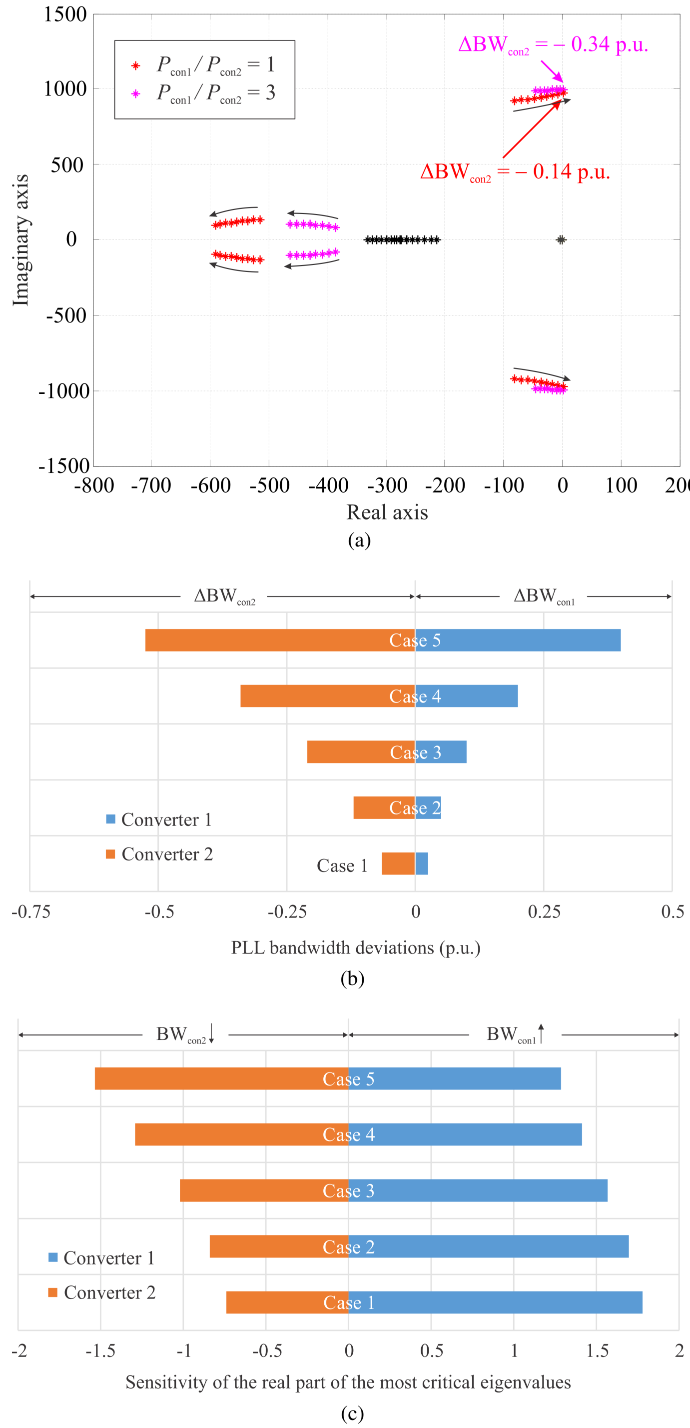

Fig. 11. Stability analysis of two PLL-synchronized converters with different power setpoints ($P_{con1}/P_{con2} = 3$) when varying PLL bandwidths: (a) eigenvalue trajectories, (b) critical PLL bandwidths of two converters, and (c) sensitivity analysis of the real part of the most critical modes to PLL bandwidth variation.

is done and the eigenvalue trajectory is shown by magenta in Fig. 11a. Here, P_{con1} and P_{con2} are the power setpoints of Converter 1 and Converter 2, respectively. The SCR of the grid is 3.5. If BW_{con1} is 0.2 p.u. higher than $BW_{limit,2p.u.}$, it can be seen in Fig. 11a that BW_{con2} has to be at least 0.34 p.u. lower than $BW_{limit,2p.u.}$ to maintain stability. For comparison, the eigenvalue trajectory of converters with identical power setpoint (i.e., $P_{con1}/P_{con2} = 1$) is shown by red in the same figure. Obviously, the critical modes of converters with identical power injection are further away from the imaginary axis. Moreover, the critical PLL bandwidth of Converter 2 would be higher under this circumstance since BW_{con2} just needs to be 0.14 p.u. lower than $BW_{limit,2p.u.}$ to guarantee system stability.

This article has been accepted for publication in a future issue of this journal, but has not been fully edited. Content may change prior to final publication. Citation information: DOI 10.1109/TIA.2021.3081611, IEEE Transactions on Industry Applications

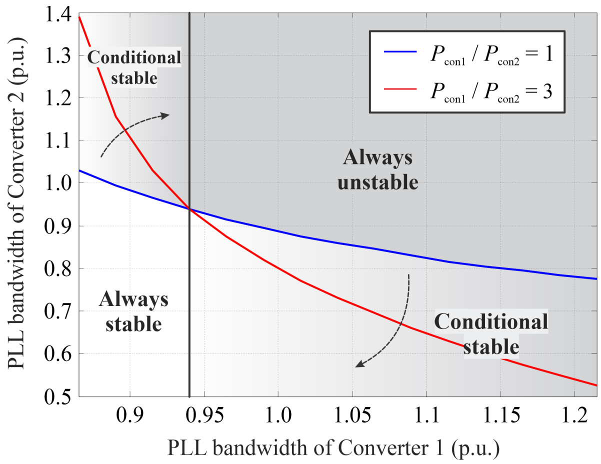

Fig. 12. Stable border of two grid converters with different power rating and PLL bandwidths.

The map of the critical PLL bandwidths for two grid converters with different power setpoints ($P_{con1}/P_{con2} = 3$) based on the eigenvalue analysis of five case studies, is presented in Fig. 11b. In contrast to Fig. 10b, it can be seen that the the critical bandwidths present asymmetric feature when the bandwidth deviations are lower, while they tend to be symmetric when the bandwidth deviations are getting higher. Sensitivity analysis of the five case studies are carried out and the sensitivity of the real parts of the critical modes to the PLL bandwidth variations are illustrated in Fig. 11c. When the bandwidth deviations are low, for instance in case 1, the absolute sensitivity values of Converter 1 is much higher than that of Converter 2, indicating much more bandwidth reduction of Converter 2 is required to maintain stability. When the bandwidth deviations are high, for example in case 5, the absolute sensitivity values of both converters are relatively close, leading to symmetric feature of critical PLL bandwidths.

To sum up, a general stability indices of critical PLL bandwidths of two grid converters can be obtained based on the above-mentioned analysis, and shown in Fig. 12. The black vertical curve indicates $BW_{limit,2p.u.}$, the blue and the red curves represent the critical PLL bandwidths of the two grid converters with identical and different power setpoints, respectively. The formal stability regions can be defined based on the blue and the black curves, where the system is always stable or unstable if the PLL bandwidths of the two converters fall into the corresponding region in the figure. Except the always stable and unstable regions, the stability of the rest regions relies on the ratio between P_{con1} and P_{con2}. It can be seen that the stable border can be extended, rotating clockwise when the ratio between P_{con1} and P_{con2} increases, till the vertical curve $BW_{limit,2p.u.}$, namely, $P_{con1}/P_{con2} \to +\infty$.

IV. Monte-Carlo Analysis

For an actual system, such as wind/solar farms, it is computationally expensive to predict the system stability considering the parameter uncertainties. Therefore, Monte-Carlo analysis has to be taken into account, which is a stochastic method to address the problem. Several case studies have been done based on the Monte-Carlo analysis and the results are illustrated in Fig. 13 and Fig. 14. In all the case studies, the values of the real parts of the critical modes are considered as the stability index.

Firstly, the probability distributions of the most critical modes of grid converter(s) under different SCR are studied in Fig. 13a. The probability distributions from left to right refer to the SCR varying from 5 to 1.5. It can be seen that the probability distribution are gradually moves to the positive half plane when the SCR becomes lower, namely, the grid becomes weaker, indicating the system becomes unstable in a weak grid. Especially when the SCR equals to 1.5, the majority of the probability distribution locates in the unstable region.

Secondly, the probability distributions of the most critical modes of PLL-synchronized converter(s) with different PLL bandwidths and different power setpoints when SCR is 3 are studied. The probability distributions are presented in Fig. 13b and Fig. 13c, respectively. In Fig. 13b, the probability distributions from left to right refer to the PLL bandwidth varying from 100 Hz to 300 Hz. In Fig. 13c, the probability distributions from left to right refer to the power setpoint varying from 0.5 p.u. to 1 p.u.. For the two case studies, it can be seen that the probability distribution moves towards right half plane when increasing either the PLL bandwidth or the power setpoint/injection.

Then, the Monte-Carlo analysis of the most critical modes of two converters with same power setpoint while different PLL bandwidths are investigated, and the probability distributions of three scenarios are presented in Fig. 14a. In the first scenario, bandwidth of both converters equals to $BW_{limit,2p.u.}$, thus $\Delta BW_{con1} = \Delta BW_{con2} = 0$ Hz, and the distribution is indicated by the blue bars. In the second scenario, the deviations between the PLL bandwidths and $BW_{limit,2p.u.}$ are: ΔBW_{con1} = +20 Hz, $\Delta BW_{con2} = -20$ Hz, and the distribution is shown by the green bars. It can be seen that the distribution of the second scenario is nearly overlapping with the one of the first scenario, indicating the stability conditions are similar. This is due to the fact that the absolute values of the sensitivity of the two converters are very close when the deviations are low, according to Fig. 10c, thus the critical modes do not move. When the deviations between the PLL bandwidths and $BW_{limit,2p.u.}$ become higher, e.g., ΔBW_{con1} = +100 Hz, $\Delta BW_{con2} = -100$ Hz in the third scenario, the distribution is shown by the yellow bars and moves towards more stable region. This is because the absolute value of the sensitivity of the converter decreasing bandwidth is much higher than that of the converter increasing bandwidth when the deviations are high, according to Fig. 10c, leading the critical modes to move leftwards.

In Fig. 14b, the probability distributions of the most critical modes of two converters with different PLL bandwidths and different power setpoints (e.g., $P_{con1}/P_{con2} = 2$) are investigated. In the first scenario, bandwidth of both converters equals to $BW_{limit,2p.u.}$, and the distribution is indicated by the blue bars. In the second scenario, the deviations between the PLL bandwidths and $BW_{limit,2p.u.}$ are: ΔBW_{con1} = +20 Hz, $\Delta BW_{con2} = -20$ Hz, and the distribution is shown by the green bars. Comparing to the distribution of the first scenario,

This article has been accepted for publication in a future issue of this journal, but has not been fully edited. Content may change prior to final publication. Citation information: DOI 10.1109/TIA.2021.3081611, IEEE Transactions on Industry Applications

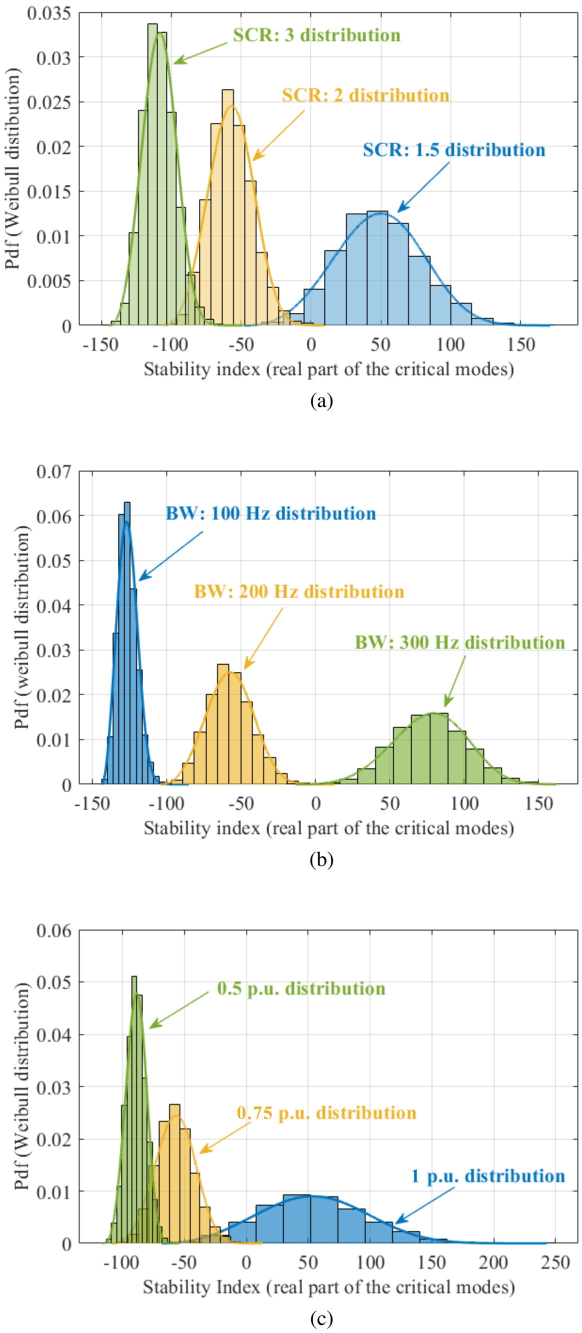

Fig. 13. Monte-Carlo analysis of grid converters considering their synchronization: (a) with different SCRs, (b) with different PLL bandwidths, and (c) with different power setpoints.

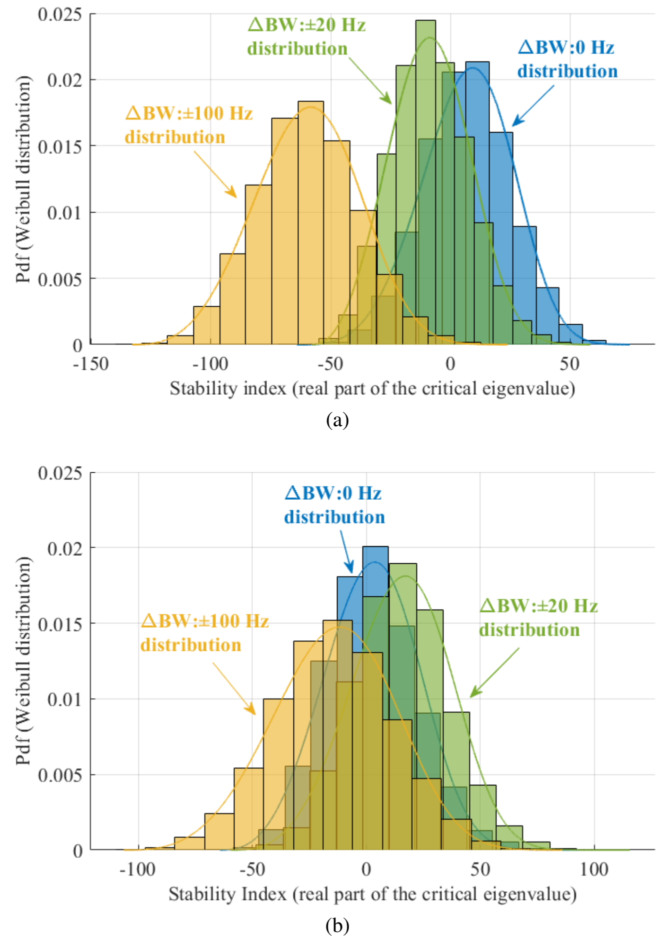

Fig. 14. Monte-Carlo analysis of two grid converters: (a) with same power setpoint and (b) with different power setpoints ($P_{con1}/P_{con2} = 2$).

the distribution of the second scenario moves to the less stable region. The reason is that the absolute value of the sensitivity of the converter with high power injection is much higher than that of the converter with low power injection when the bandwidth deviations are low, according to Fig. 11c. This leads to the critical modes moving rightwards. In the third scenario, the deviations between the PLL bandwidths and $BW_{limit,2p.u.}$ further increase: ΔBW_{con1} = +100 Hz, $\Delta BW_{con2} = -100$ Hz, the distribution is shown by the yellow bars. Comparing to the distributions of the previous two scenarios, this distribution moves towards the more stable region and is almost overlapping with the one of the first scenario. This is due to the fact that the absolute values of the sensitivity of the two converters are pretty close according to Fig. 11c, and therefore leading to the critical modes being at the original locations as those of the first scenario.

V. Experimental Validation

To validate the effectiveness, laboratory setup with two grid converters has been built as shown in Fig. 15a and the analysis has been tested experimentally. The detailed system configuration is presented in Fig. 15b. The PCC voltage is supplied by the connection to centralized power plant, being emulated by a real-time digital simulator (RTDS), and a Spitzenberger PAS series of 4-quadrant power amplifier provides the interface to the converters, which are two Danfoss FC302 converters The control strategy as well as the synchronization of grid converter (as shown in Fig. 1b) has been implemented in a dSPACE 1006 processor board. The sampling frequency of 10 kHz is used for the overall control system. For the sake of convenience and synchronization, the control of both grid converters have been achieved by the same dSPACE processor board.

The PCC voltage and converter current waveforms (phase A) when the PLL bandwidth(s) varying from its stable region

This article has been accepted for publication in a future issue of this journal, but has not been fully edited. Content may change prior to final publication. Citation information: DOI 10.1109/TIA.2021.3081611, IEEE Transactions on Industry Applications

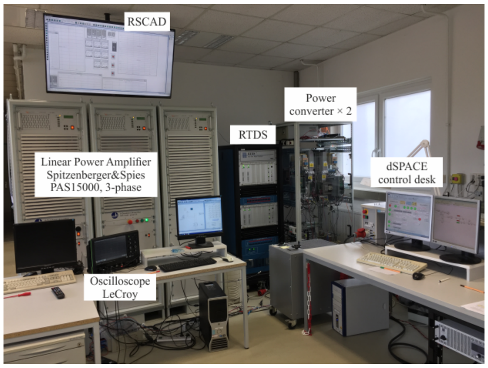

(a)

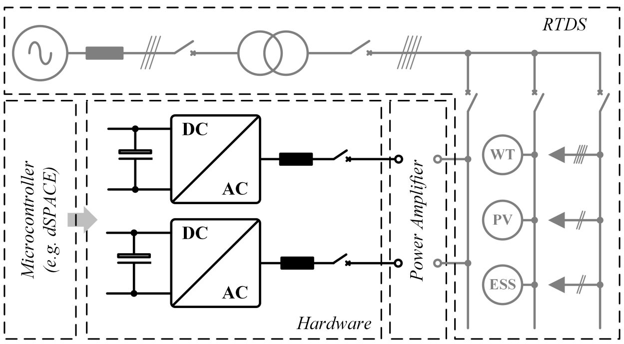

(b)

Fig. 15. Experimental setup: (a) photo and (b) system configuration.

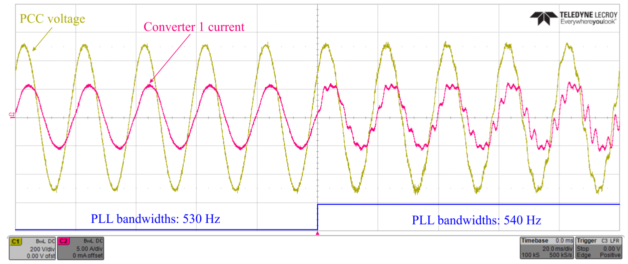

(a)

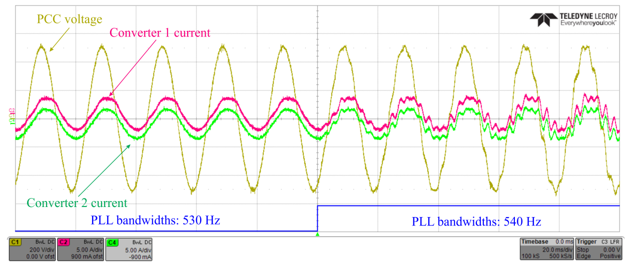

(b)

Fig. 16. Experimental waveforms during PLL bandwidth variation (Time: 20 ms/div, PCC voltage: 200 V/div, Converter current: 5 A/div): (a) single converter with power setpoint 2.5 kW and (b) two converters with total power setpoint 2.5 kW.

to the critical one are shown in Fig. 16. For both case studies, the PLL bandwidth jumps from 530 Hz to 540 Hz. The power setpoint/injection of the single grid converter of Fig. 16a equals to the total power setpoint/injection of the two grid converters of Fig. 16b, which is 2.5 kW. It can be seen that instability in terms of oscillations and harmonic distortions occur in both cases, when the PLL bandwidth reaches 540 Hz. Obviously, the critical PLL bandwidths of the both cases are the same since the total power injections are identical.

The stability border regarding SCR and critical PLL bandwidth of grid converter(s) is obtained by the experimental results, as shown by the red crosses in Fig. 17. For comparison, the stability border of Fig. 9, obtaining from the developed model, is presented in the figure by the blue solid line. It can be seen that the experimental results well match the numerical analysis obtained by the developed model.

The experimental results of two grid converters with different PLL bandwidths are carried out, where the waveforms of two case studies are shown in Fig. 18. The power injections of the both converters are 2.5 kW and the total power injection is identical to that of the previous case studies given in Fig. 16. Therefore, the previous critical PLL bandwidth $BW_{limit,2p.u.}$ 540 Hz is still valid for the following tests.

In Fig. 18a, it can be seen that the system becomes unstable when the two PLL bandwidths reach to 510 Hz and 570 Hz, respectively. The deviations between the PLL bandwidths and $BW_{limit,2p.u.}$ are: $\Delta BW_{con1} = -30$ Hz, $\Delta BW_{con2} = +30$ Hz, showing that critical bandwidths turn out to be symmetric to $BW_{limit,2p.u.}$. When higher bandwidth deviations are applied, as shown in Fig. 18b, it can be seen that the system

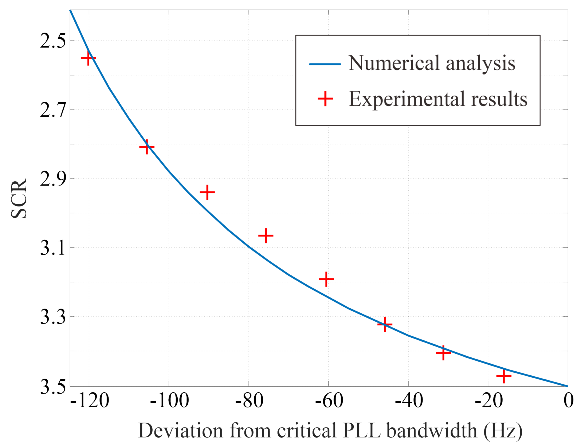

Fig. 17. Stability borders of grid converter(s) obtained from developed model (solid blue curve) and experimental results (red crosses).

becomes unstable when the two PLL bandwidths reach to 445 Hz and 760 Hz, respectively. The deviations between the PLL bandwidths and $BW_{limit,2p.u.}$ are: $\Delta BW_{con1} = -95$ Hz, $\Delta BW_{con2} = +220$ Hz. Obviously, the critical bandwidths present an asymmetric behavior to $BW_{limit,2p.u.}$. Moreover, it can be seen that higher frequency oscillations occur at the unstable stage when the bandwidth deviations become higher. This is due to the critical modes moving to the higher frequency when higher bandwidth deviations are applied, as illustrated in Fig. 10a.

To plot the full map of the critical bandwidths for stable operation, five case studies of two grid converters with different PLL bandwidths are evaluated experimentally. The full map is shown in Fig. 19a. For all the five case studies, the power setpoints of both converters are 2.5 kW and $BW_{limit,2p.u.}$ is 540 Hz. Comparing to the map obtained from the developed

This article has been accepted for publication in a future issue of this journal, but has not been fully edited. Content may change prior to final publication. Citation information: DOI 10.1109/TIA.2021.3081611, IEEE Transactions on Industry Applications

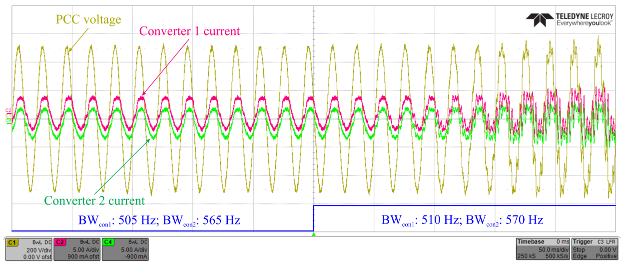

(a)

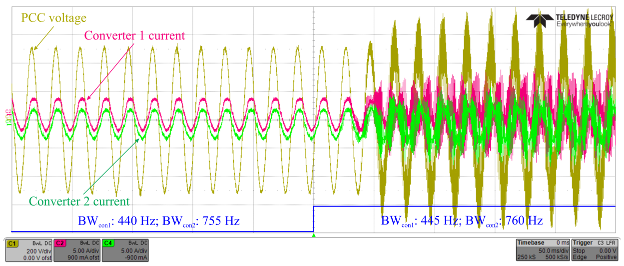

(b)

Fig. 18. Experimental waveforms of two converters with equal power setpoint 2.5 kW and different PLL bandwidths (Time: 50 ms/div, PCC voltage: 200 V/div, Converter current: 5 A/div): (a) BW_{con1} = 505 Hz, BW_{con2} = 565 Hz and (b) BW_{con1} = 440 Hz, BW_{con2} = 755 Hz.

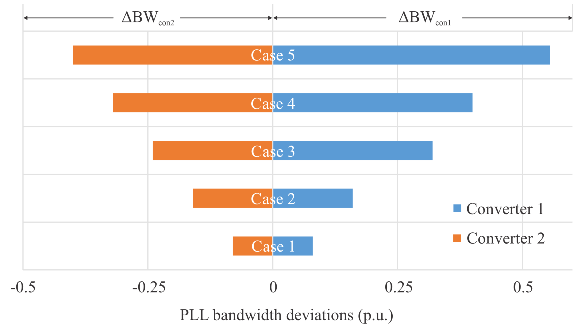

(a)

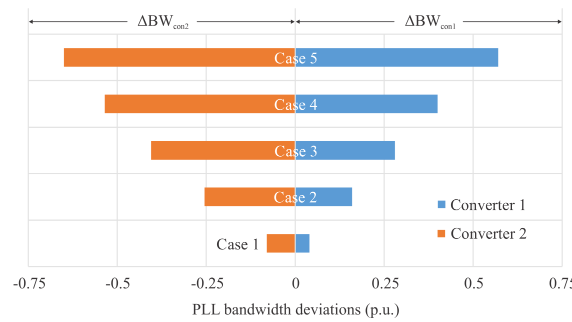

(b)

Fig. 19. Experimental results of stability limits of two grid converters: (a) with same power setpoint and (b) with different power setpoints ($P_{con1}/P_{con2} = 3$).

model (as shown in Fig. 10b), the map obtained experimentally presents similar characteristics: the critical bandwidths are symmetric when the bandwidth deviations are low, while they become asymmetric when the bandwidth deviations are higher.

The critical PLL bandwidths for two grid converters with different power setpoints are also studied experimentally. The full map of the critical bandwidths is shown in Fig. 19b. For all the five case studies, the total amount of power injection of the two converters is 5 kW ($P_{con1}/P_{con2} = 3$) and therefore $BW_{limit,2p.u.}$ is still 540 Hz. Comparing to the map obtained from the developed model (as shown in Fig. 11b), the experimental one presents similar characteristics: the critical bandwidths are asymmetric when the bandwidth deviations are low, while they tend to be symmetric when the bandwidth deviations are getting higher.

VI. Conclusions

This paper studies the stability issues of two PLL-synchronized grid converters with different bandwidths and different power setpoints in a weak grid. A CCM-based state-space model including grid converters and LV network has been developed in the paper. The eigenvalue analysis for several scenarios have been carried out using the developed model. According to the eigenvalue analysis, conclusions for the two PLL-synchronized grid converters can be drawn as follows:

- Critical PLL bandwidth depends on the power setpoints of converters or the SCR of grid;
- when the PLL bandwidth of one converter exceed the critical bandwidth, one can reduce the PLL bandwidth of another converter to guarantee the stability of both converters, and vice versa;
- when the power setpoints are different, the PLL bandwidth of the converter with higher power setpoint can be tuned to achieve stable operation of both converters in a more effective way.

Moreover, stability maps/indices of the two PLL-synchronized converters have been plotted based on the analysis. Monte-Carlo analysis and experimental results have been provided to validate the effectiveness of the theoretical analysis. The conclusions as well as the stability maps/indices of the two-converter system can be further extended to two wind/solar farms in the distribution grids. In particular, when one wind/solar farm has been installed, to install another one connected to the same PCC, the power setpoints and the PLL bandwidth of the converters for another one should be dedicatedly designed following the stability border shown in Fig. 12 to ensure stable operation of both farms.

Besides, due to the increasing penetration of renewables, it is necessary to determine the interactions among N converters and their effects on the utility. Future work on this topic includes modeling and cluster, methodology of interaction analysis, stability criteria can be studied to provide a more general design guideline for the wind/solar farms.

Appendix

The differential equations of grid converters (referring to (5)) are listed in the followings.

The state equations of the measured PCC voltages in dq

frame:

$$\begin{aligned}\frac{\mathrm{d}v^m_{PCC,d}}{\mathrm{d}t} =& -v^m_{PCC,d} + v^m_{PCC,q}(k_p^{PLL}v^m_{PCC,q} + k_i^{PLL}\gamma) \\ &+ v_{PCC,d}cos\Delta\theta + v_{PCC,q}sin\Delta\theta;\end{aligned} \tag{14}$$

$$\begin{aligned}\frac{\mathrm{d}v^m_{PCC,q}}{\mathrm{d}t} =& -v^m_{PCC,q} + v^m_{PCC,d}(k_p^{PLL}v^m_{PCC,q} + k_i^{PLL}\gamma) \\ &- v_{PCC,d}sin\Delta\theta + v_{PCC,q}cos\Delta\theta.\end{aligned} \tag{15}$$

The state equation of the phase deviation:

$$\frac{\mathrm{d}\Delta\theta}{\mathrm{d}t} = k_p^{PLL}v^m_{PCC,q} + k_i^{PLL}\gamma. \tag{16}$$

The state equation of the integrator of the PI of the SRF-PLL:

$$\frac{\mathrm{d}\gamma}{\mathrm{d}t} = v^m_{PCC,q}. \tag{17}$$

The state equations of the PI controllers for current control in dq frame:

$$\frac{\mathrm{d}e_d}{\mathrm{d}t} = I_{ref,d} - i^m_{con,d}; \tag{18}$$

$$\frac{\mathrm{d}e_q}{\mathrm{d}t} = I_{ref,q} - i^m_{con,q}. \tag{19}$$

The state equations of the measured converter currents in dq frame:

$$\begin{aligned}\frac{\mathrm{d}i^m_{con,d}}{\mathrm{d}t} =& -i^m_{con,d} + i^m_{con,q}(k_p^{PLL}v^m_{PCC,q} + k_i^{PLL}\gamma) \\ &+ i_{con,d}cos\Delta\theta + i_{con,q}sin\Delta\theta;\end{aligned} \tag{20}$$

$$\begin{aligned}\frac{\mathrm{d}i^m_{con,q}}{\mathrm{d}t} =& -i^m_{con,q} + i^m_{con,d}(k_p^{PLL}v^m_{PCC,q} + k_i^{PLL}\gamma) \\ &- i_{con,d}sin\Delta\theta + i_{con,q}cos\Delta\theta.\end{aligned} \tag{21}$$

The state equations of the voltage references in dq frame:

$$\begin{aligned}\frac{\mathrm{d}v_{r,d}}{\mathrm{d}t} =& \frac{cos\Delta\theta}{1.5T_s}[-L_f i^m_{con,q}(k_p^{PLL}v^m_{PCC,q} + k_i^{PLL}\gamma) \\ &+ k^{cc}_{p,d}(I_{ref,d} - i^m_{con,d}) + k^{cc}_{i,d}e_d + v^m_{PCC,d}] \\ &- \frac{sin\Delta\theta}{1.5T_s}[-L_f i^m_{con,d}(k_p^{PLL}v^m_{PCC,q} + k_i^{PLL}\gamma) \\ &+ k^{cc}_{p,q}(I_{ref,q} - i^m_{con,q}) + k^{cc}_{i,q}e_q + v^m_{PCC,q}] \\ &- \frac{v_{r,d}}{1.5T_s} - v_{r,q}(k_p^{PLL}v^m_{PCC,q} + k_i^{PLL}\gamma);\end{aligned} \tag{22}$$

$$\begin{aligned}\frac{\mathrm{d}v_{r,q}}{\mathrm{d}t} =& \frac{sin\Delta\theta}{1.5T_s}[-L_f i^m_{con,q}(k_p^{PLL}v^m_{PCC,q} + k_i^{PLL}\gamma) \\ &+ k^{cc}_{p,d}(I_{ref,d} - i^m_{con,d}) + k^{cc}_{i,d}e_d + v^m_{PCC,d}] \\ &+ \frac{cos\Delta\theta}{1.5T_s}[-L_f i^m_{con,d}(k_p^{PLL}v^m_{PCC,q} + k_i^{PLL}\gamma) \\ &+ k^{cc}_{p,q}(I_{ref,q} - i^m_{con,q}) + k^{cc}_{i,q}e_q + v^m_{PCC,q}] \\ &- \frac{v_{r,d}}{1.5T_s} - v_{r,d}(k_p^{PLL}v^m_{PCC,q} + k_i^{PLL}\gamma).\end{aligned} \tag{23}$$

The state equations of the actual injected currents in dq frame:

$$\begin{aligned}\frac{\mathrm{d}i_{con,d}}{\mathrm{d}t} =& i_{con,q}(k_p^{PLL}v^m_{PCC,q} + k_i^{PLL}\gamma) \\ &+ \frac{1}{L_f}(-v_{PCC,d} + v_{r,d} - i_{con,d}R_f);\end{aligned} \tag{24}$$

$$\begin{aligned}\frac{\mathrm{d}i_{con,q}}{\mathrm{d}t} =& i_{con,d}(k_p^{PLL}v^m_{PCC,q} + k_i^{PLL}\gamma) \\ &+ \frac{1}{L_f}(-v_{PCC,q} + v_{r,q} - i_{con,q}R_f).\end{aligned} \tag{25}$$

The differential equations of LV network (referring to (6)) are listed in the followings.

The state equation of the PCC voltage:

$$\frac{\mathrm{d}v_{PCC}}{\mathrm{d}t} = \frac{1}{C_L}i_{conj} - \frac{1}{C_L}i_g - \frac{1}{C_L}i_L. \tag{26}$$

The state equation of the grid current:

$$\frac{\mathrm{d}i_g}{\mathrm{d}t} = \frac{1}{L_g}v_{PCC} - \frac{1}{L_g}v_g - \frac{R_g}{L_g}i_g. \tag{27}$$

The state equation of the load current:

$$\frac{\mathrm{d}i_L}{\mathrm{d}t} = \frac{1}{L_L}v_{PCC} - \frac{R_L}{L_L}i_L. \tag{28}$$

The authors would like to thank...

REFERENCES

[1] F. Blaabjerg, R. Teodorescu, M. Liserre, and A. V. Timbus, "Overview of control and grid synchronization for distributed power generation systems," *IEEE Trans. Ind. Electron.*, vol. 53, no. 5, pp. 1398–1409, 2006.

[2] Z. Zou and M. Liserre, "Modeling phase-locked loop-based synchronization in grid-interfaced converters," *IEEE Transactions on Energy Conversion*, vol. 35, no. 1, pp. 394–404, 2020.

[3] Z. Zou, G. Buticchi, M. Liserre, A. M. Kettner, and M. Paolone, "Voltage stability analysis using a complete model of grid-connected voltage-source converters," in *IEEE Energy Conversion Congress and Exposition (ECCE)*, Sept 2016, pp. 1–8.

[4] G. Buticchi, G. D. Carne, D. Barater, Z. Zou, and M. Liserre, "Analysis of the frequency-based control of a master/slave micro-grid," *IET Renewable Power Generation*, vol. 10, no. 10, pp. 1570–1576, 2016.

[5] J. Sun, "Small-signal methods for ac distributed power systems - a review," *IEEE Transactions on Power Electronics*, vol. 24, no. 11, pp. 2545–2554, 2009.

[6] L. Harnefors, M. Bongiorno, and S. Lundberg, "Input-admittance calculation and shaping for controlled voltage-source converters," *IEEE Transactions on Industrial Electronics*, vol. 54, no. 6, pp. 3323–3334, Dec 2007.

[7] B. Wen, D. Boroyevich, R. Burgos, P. Mattavelli, and Z. Shen, "Analysis of d-q small-signal impedance of grid-tied inverters," *IEEE Transactions on Power Electronics*, vol. 31, no. 1, pp. 675–687, Jan 2016.

[8] X. Wang, L. Harnefors, and F. Blaabjerg, "Unified impedance model of grid-connected voltage-source converters," *IEEE Transactions on Power Electronics*, vol. 33, no. 2, pp. 1775–1787, 2018.

[9] Y. Liao, Z. Liu, H. Zhang, and B. Wen, "Low-frequency stability analysis of single-phase system with dq-frame impedance approach part i impedance modeling and verification," *IEEE Transactions on Industry Applications*, vol. 54, no. 5, pp. 4999–5011, 2018.

[10] S. Golestan, M. Monfared, and F. D. Freijedo, "Design-oriented study of advanced synchronous reference frame phase-locked loops," *IEEE Transactions on Power Electronics*, vol. 28, no. 2, pp. 765–778, 2013.

[11] X. Zhang, D. Xia, Z. Fu, G. Wang, and D. Xu, "An improved feedforward control method considering pll dynamics to improve weak grid stability of grid-connected inverters," *IEEE Transactions on Industry Applications*, vol. 54, no. 5, pp. 5143–5151, 2018.

[12] D. Zhu, S. Zhou, X. Zou, and Y. Kang, "Improved design of pll controller for lcl-type grid-connected converter in weak grid," *IEEE Transactions on Power Electronics*, vol. 35, no. 5, pp. 4715–4727, 2020.

[13] Z. Zou, R. Rosso, and M. Liserre, "Modeling of the phase detector of a synchronous-reference-frame phase-locked loop based on second-order approximation," *IEEE Journal of Emerging and Selected Topics in Power Electronics*, vol. 8, no. 3, pp. 2534–2545, 2020.

[14] H. Wu and X. Wang, "Design-oriented transient stability analysis of pll-synchronized voltage-source converters," *IEEE Transactions on Power Electronics*, vol. 35, no. 4, pp. 3573–3589, 2020.

[15] P. Kundur, *Power System Stability and Control*. McGraw-Hill, Inc., 1994.

[16] X. Wang and F. Blaabjerg, "Harmonic stability in power electronic-based power systems: Concept, modeling, and analysis," *IEEE Transactions on Smart Grid*, vol. 10, no. 3, pp. 2858–2870, 2019.

[17] G. Gaba, S. Lefebvre, and D. Mukhedkar, "Comparative analysis and study of the dynamic stability of ac/dc systems," *IEEE Transactions on Power Systems*, vol. 3, no. 3, pp. 978–985, Aug 1988.

[18] S. Arabi, G. J. Rogers, D. Y. Wong, P. Kundur, and M. G. Lauby, "Small signal stability program analysis of svc and hvdc in ac power systems," *IEEE Transactions on Power Systems*, vol. 6, no. 3, pp. 1147–1153, Aug 1991.

[19] Y. Wang, X. Wang, F. Blaabjerg, and Z. Chen, "Harmonic instability assessment using state-space modeling and participation analysis in inverter-fed power systems," *IEEE Transactions on Industrial Electronics*, vol. 64, no. 1, pp. 806–816, 2017.

[20] Y. Wang, X. Wang, Z. Chen, and F. Blaabjerg, "Small-signal stability analysis of inverter-fed power systems using component connection method," *IEEE Transactions on Smart Grid*, vol. 9, no. 5, pp. 5301–5310, Sep. 2018.

[21] R. Rosso, S. Engelken, and M. Liserre, "Robust stability analysis of synchronverters operating in parallel," *IEEE Transactions on Power Electronics*, vol. 34, no. 11, pp. 11 309–11 319, 2019.

[22] ——, "Robust stability investigation of the interactions among grid-forming and grid-following converters," *IEEE Journal of Emerging and Selected Topics in Power Electronics*, vol. 8, no. 2, pp. 991–1003, 2020.

[23] R. Rosso, G. Buticchi, M. Liserre, Z. Zou, and S. Engelken, "Stability analysis of synchronization of parallel power converters," in *43rd Annual Conference of the IEEE Industrial Electronics Society*, Oct 2017, pp. 440–445.

[24] R. Rosso, M. Andresen, S. Engelken, and M. Liserre, "Analysis of the interaction among power converters through their synchronization mechanism," *IEEE Transactions on Power Electronics*, vol. 34, no. 12, pp. 12 321–12 332, 2019.

[25] Jung-Won Kim, Hang-Seok Choi, and Bo Hyung Cho, "A novel droop method for converter parallel operation," *IEEE Transactions on Power Electronics*, vol. 17, no. 1, pp. 25–32, Jan 2002.

[26] Z. Zou, B. D. Besheli, R. Rosso, and M. Liserre, "Interactions between phase-locked loop synchronized grid converters with different bandwidths and power ratings," in *IEEE Energy Conversion Congress and Exposition (ECCE)*, 2019, pp. 5430–5437.

[27] F. Blaabjerg, R. Teodorescu, M. Liserre, and A. V. Timbus, "Overview of control and grid synchronization for distributed power generation systems," *IEEE Transactions on Industrial Electronics*, vol. 53, no. 5, pp. 1398–1409, 2006.

[28] L. F. Drbal, P. G. Boston, and K. L. Westra, *Power Plant Engineering*. Boston, MA, USA: Springer, 1996.

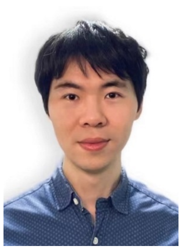

Zhixiang Zou (S'12-M'18-SM'20) received the B.Eng. and Ph.D. degrees in electrical and engineering from Southeast University, Nanjing, China, in 2007 and 2014, respectively, the Dr.-Ing. degree (summa cum laude) from Kiel University, Germany, in 2019. He was an engineer in the State Grid Electric Power Research Institute, Nanjing, China, from 2007 to 2009. He was a research fellow at the Chair of Power Electronics, Kiel University, Germany, from 2014 to 2019. He is now an associate professor in the School of Electrical Engineering at the Southeast University. His research interests include smart transformers, microgrid stability, modeling and control of power converters.

Dr. Zou serves as an Associate Editor of the IEEE Open Journal of Power Electronics, an Associate Editor of the IEEE Access, an Editor of the International Transactions on Electrical Energy Systems, and an Editor of the Mathematical Problem in Engineering, and a Standing Director of IEEE PES Power System Relaying & Control Satellite Committee.

Behnam Daftary Besheli received the B.Eng in electrical engineering with the branch of control engineering in K.N. Toosi University of Technology, Tehran, Iran in 2004. He was an automation system designer and programmer in the field of automation systems, Instrumentation in the offshore/onshore Oil and Gas industry in Iran from 2005 to 2013. He received his M.Eng in electrical engineering in the Christian-Albrecht University of Kiel, Germany in 2019. He is now the head of electrical department in the LAWI Engineering GmbH, active in designing the electrical systems, automation and instrumentation of Biomass fuel thermal power plants. Currently, he is a guest researcher and cooperating with the power electronics department in Christian-Albrecht University of Kiel.

Roberto Rosso (S'17) received the B.Sc. degree in electronic engineering and the M.Sc. degree in electrical engineering in 2009 and 2012, respectively, from the University of Catania, Catania, Italy. He is currently working toward the Ph.D. degree (since 2017) in electrical engineering at the Christian-Albrechts-University of Kiel, Kiel, Germany.

In 2013, he joined the R&D division of the wind turbine manufacture ENERCON (Wobben Research and Development WRD), where he is currently working at the Control Engineering Department. He has been involved in several research projects addressing analytical models of electrical machines, control of electric drive systems, and control of grid-connected converters, contributing as inventor and co-inventor to several patents held by the company.

His research interests include converter control strategies for grid integration in systems with high penetration of power electronics-based power sources. He is member of the Workgroup GC0137 established by the British System Operator NGESO on minimum specification required for provision of GB grid forming capability.

Marco Liserre (S'00-M'02-SM'07-F'13) received the MSc and PhD degree in Electrical Engineering from the Bari Polytechnic, respectively in 1998 and 2002. He has been Associate Professor at Bari Polytechnic and from 2012 Professor in reliable power electronics at Aalborg University (Denmark). From 2013 he is Full Professor and he holds the Chair of Power Electronics at Kiel University (Germany). He has published 500 technical papers (1/3 of them in international peer-reviewed journals) and a book. These works have received more than 35000 citations. Marco Liserre is listed in ISI Thomson report "The world's most influential scientific minds" from 2014 and in Clarivate Analytics report "Highly Cited Researchers" from 2020.

He has been awarded with an ERC Consolidator Grant for the project "The Highly Efficient And Reliable smart Transformer (HEART), a new Heart for the Electric Distribution System".

He is member of IAS, PELS, PES and IES. He has been serving all these societies in different capacities. He has received the IES 2009 Early Career Award, the IES 2011 Anthony J. Hornfeck Service Award, the 2014 Dr. Bimal Bose Energy Systems Award, the 2011 Industrial Electronics Magazine best paper award and the Third Prize paper award by the Industrial Power Converter Committee at ECCE 2012, 2012, 2017 IEEE PELS Sustainable Energy Systems Technical Achievement Award and the 2018 IEEE-IES Mittelmann Achievement Award.

Xiongfei Wang (S'10-M'13-SM'17) received the B.S. degree from Yanshan University, Qinhuangdao, China, in 2006, the M.S. degree from Harbin Institute of Technology, Harbin, China, in 2008, both in electrical engineering, and the Ph.D. degree in energy technology from Aalborg University, Aalborg, Denmark, in 2013.

From 2009 he has been with the Department of Energy Technology, Aalborg University, where he became an Assistant Professor in 2014, an Associate Professor in 2016, a Professor and Leader of Electronic Power Grid (eGrid) Research Group in 2018. He is also a part-time Professor of KTH Royal Institute of Technology, Stockholm, Sweden, from 2020. His current research interests include dynamic analysis and control of power electronic converters and systems, power electronics for sustainable energy systems and electrical grids, high power converters and multi-converter systems.

Dr. Wang serves as a Member-at-Large of Administrative Committee for the IEEE Power Electronics Society (PELS) in 2020-2022, a Co-Editor-in-Chief for the IEEE TRANSACTIONS ON POWER ELECTRONICS, and as an Associate Editor for the IEEE JOURNAL OF EMERGING AND SELECTED TOPICS IN POWER ELECTRONICS. He was selected into Aalborg University Strategic Talent Management Program in 2016. He has received six Prize Paper Awards in the IEEE Transactions and conferences, the 2016 Outstanding Reviewer Award of IEEE TRANSACTIONS ON POWER ELECTRONICS, the 2018 Richard M. Bass Outstanding Young Power Electronics Engineer Award from the IEEE PELS, the 2019 IEEE PELS Sustainable Energy Systems Technical Achievement Award, the 2020 IEEE Power & Energy Society Prize Paper Award, and the Highly Cited Researcher in the Web of Science in 2019-2020.